# OPTIMAL DATA-DRIVEN DIFFERENCE-INVERSION-BASED ITERATIVE CONTROL: HIGH-SPEED NANOPOSITIONING TRACKING EXAMPLE

Zezhou Zhang, Qingze Zou

Abstract-In this paper, an optimal data-driven difference-inversion-based iterative control (ODDD-IIC) method is proposed for high-speed precision tracking in the presence of dynamics changes and random disturbances. Iterative learning control (ILC) has been shown advantageous over feedback and feedforward control for repetitive operations. Challenges, however, still exist to achieve high accuracy and fast convergence in ILCs as the bandwidth, i.e., the frequency range for guaranteed convergence, can be limited by adverse effects of modeling error and random disturbances. The aim of the proposed method is to compensate for these adverse effects through a data-driven approach without modeling process. A frequency- and iteration- dependent iteration gain is introduced in the control law to enhance both the tracking performance and the robustness. The technique is illustrated in the experiment on output tracking of a piezoelectric actuator, with comparison to two existing ILC methods.

Index Terms— data-driven, iterative learning control, system inversion, nanopositioning control

#### I. INTRODUCTION

IGH-SPEED precision output tracking has been increasingly needed in various control applications, ranging from semiconductor manufacturing [1], nanopositioning [2], 3D-printing [3], to robot manipulation [4]. In these applications, precision tracking of the desired trajectory (contour) in repetitive operations at high-speed is critical, even in the presence of system dynamics changes and model uncertainties. Compared to feedback control where fundamental constraints are imposed by non-minimum phase zeros [5] and bandwidth robustness trade-off [6], and feedforward control that can be sensitive to model uncertainties and external disturbances [7], iterative learning control (ILC) provides an effective avenue to fully exploit both the repetition, the knowledge of system dynamics [8], [9], and the input-output data [10], [11] for output tracking. Limitations, however, exist in current ILC techniques in modeling, robustness against dynamics changes,

This work was supported by NSF grants CMMI-1660355, CMMI-1851097 and IIBR-1952823.

Z.Zhang and Q.Zou are with the Department of Mechanical and Aerospace Engineering, Rutgers, The State University of New Jersey, Piscataway, New Jersy, 08854 USA (e-mail: zz389@scarletmail.rutgers.edu; qzzou@soe.rutgers.edu).

and implementation efficiency (e.g., convergence rate). In this paper, we propose a data-driven ILC technique to tackle these limitations.

It is challenging to achieve high-speed precision tracking efficiently in the presence of dynamics changes. For example, knowledge of system dynamics has been exploited in the ILC framework [12]-[14] for high precision output tracking. Compared to conventional constant-gain ILCs (e.g., P-type or PD-type) [15], [16], these model-based ILCs improved the convergence rate and tracking performance at high speed. However, robustness against dynamics changes has not yet been accounted for. This robustness issue might be accounted for by designing an iteration-varying gain [17]. However, the disturbances are assumed to approach a periodic signal with the iterations—their randomness nature was not considered, nor was the convergence rate. Moreover, statespace modeling of the system dynamics is needed to design the iteration gain [17]. The need for a parameterized model can be alleviated through the development of the constrained data-driven optimal iterative learning control method [18], where the input-output data is used to tune the iteration gain to minimize the next-step error. However, the changes in the system dynamics are not considered in the convergence analysis, and between-iteration variations are not accounted for. Although the between-iteration uncertainties might be accounted for through an extended contraction mapping-based approach [19], a modeling process is still needed, and the convergence is slow (e.g., hundreds of iterations) for practice uses. Therefore, efforts are needed to achieve, in the ILC framework, high-performance and robustness, both efficiently (e.g., rapid convergence, and no need of the modeling process) and effectively (e.g., high-precision tracking at high-speed).

Recently, data-driven ILCs have been proposed to overcome the above limitations for high-speed precision tracking and robustness. Instead of using a *fixed* dynamics model or not using a model at all, in the data-driven ILCs [20]–[22], the dynamics model of the system is constructed and updated by using the input-output data along with the iteration process. Not only is the modeling process eliminated/avoided, but also the changes of the system dynamics are automatically accounted for [10], [11]. For example, a modeling-free ILC technique has been demonstrated for rapid convergence (e.g., a

handful iterations) and high-speed precision tracking in various applications [23], [24]. Alternatively, the input-output data has also been exploited to construct a finite-impulse-response (FIR)-based filter directly in the ILC algorithm [21], [25], or to adaptively tune the output-dependent control parameters to mitigate error propagation [20]. This data-driven idea has been extended to use the gradient of the input-output data [10] to further improve the tracking performance of systems with both hysteresis and dynamics effects. Therefore, the data-driven approach to ILC is promising to achieve high-speed precision tracking under adverse effects of dynamics variations and random disturbances.

In this paper, a data-driven nonlinear, time-varying ILC approach is developed. Based on the modeling-free differenceinversion-based iterative control technique [10], we propose to adjust the frequency-dependent iteration gain in each iteration. It is shown that by using the system frequency responses and the output noise acquired a priori, along with the inputoutput data measured during the iteration, the iteration gain can be adjusted to enhance both the robustness and the tracking performance: Not only is random noise of a larger size allowed, but also convergence in a large frequency is attained. Moreover, the performance of the proposed data-driven ILC can be further enhanced by optimizing the iteration gain. The proposed method is successfully implemented in a nanopositioning control experiment on a piezoelectric actuator. The experimental results demonstrate the efficacy of the proposed approach over two previous inversion-based ILC methods [10], [11].

## II. DATA-DRIVEN ITERATIVE OPTIMAL DIFFERENCE-INVERSION-BASED ITERATIVE CONTROL

In this section, we start with a brief review of the modeling-free difference-inversion-based iterative control (MFDIIC) algorithm [10], then propose the optimal data-driven difference-inversion-based iterative control (ODDD-IIC) technique.

We consider, as depicted in Fig. 1, that the system is a linear time invariant (LTI) system, and the system output in the presence of output disturbance/measurement noise is given as

$$y(j\omega) = y_{\ell}(j\omega) + y_n(j\omega) = \mathbb{G}(j\omega)u(j\omega) + y_n(j\omega), \quad (1)$$

where, respectively,  $y_{\ell}(j\omega)$  denotes the output of the LTI system,  $\mathbb{G}(j\omega) = y_{\ell}(j\omega)/u(j\omega)$  is the system frequency response (i.e., transfer function), and  $y_n(j\omega)$  is the random output disturbance (or measurement noise, see Fig. 1). We assume that:

Assumption 1: For any given desired trajectory  $y_d(j\omega)$ , there exists a set of frequencies (called the tractable frequency set below)  $\mathcal{S}_t$ , such that for any  $\omega \in \mathcal{S}_t$ , the noise to signal ratio (NSR) is bounded above by a less-than-one constant  $\varepsilon_n$ ,

$$\frac{|y_{n,k}(j\omega)|}{|y_d(j\omega)|} \le \varepsilon_n < 1, \quad \forall k.$$
 (2)

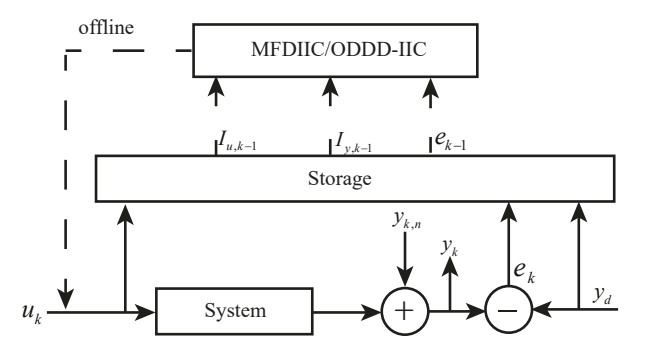


Fig. 1. The control scheme of the MFDIIC and the ODDD-IIC algorithms, where  $y_{k,n}$  is the measurement (output) noise in the  $k^{th}$  iteration,  $u_k$  is the control input for the  $k^{th}$  iteration, calculated offline by using the input-output data obtained in the  $(k-1)^{th}$  iteration ,  $I_{u,k-1}$  and  $I_{u,k-1}$ , respectively.

#### A. ODDD-IIC TECHNIQUE

The proposed ODDD-IIC method is presented in the frequency domain as follows, for any given frequency  $\omega \in \mathcal{S}_t$ :

· Initially, set

$$u_0(j\omega) = \alpha \times y_d(j\omega), \qquad k = 0,$$
  

$$u_1(j\omega) = \frac{u_0(j\omega)}{y_0(j\omega)} \times y_d(j\omega), \quad k = 1,$$
(3)

• From the  $2^{nd}$  iteration, set

$$u_{k+1}(j\omega) = \begin{cases} u_k(j\omega) + \rho_k(\omega) \frac{I_{u,k}(j\omega)}{I_{y,k}(j\omega)} \times e_k(j\omega), \\ \text{when } |\aleph_k(j\omega)| \le \eta < 1, \\ u_k(j\omega), \text{ otherwise,} \end{cases}$$
(4)

for any  $k \ge 1$ , where

$$I_{u,k}(j\omega) = u_k(j\omega) - u_{k-1}(j\omega),$$

$$I_{y,k}(j\omega) = y_k(j\omega) - y_{k-1}(j\omega),$$

$$e_k(j\omega) = y_d(j\omega) - y_k(j\omega).$$
(5)

In Eq. (4),  $\eta$  is a pre-chosen constant arbitrarily close to 1, and  $|\aleph_k(j\omega)|$  is the noise to output difference ratio (NODR) given by

$$|\aleph_k(j\omega)| = \left| \frac{\delta y_{n,k}(j\omega)}{I_{y\ell,k}(j\omega)} \right| = \left| \frac{\delta y_{n,k}(j\omega)}{\mathbb{G}I_{u,k}(j\omega)} \right|, \quad \forall k \ge 1, \quad (6)$$

where

$$\delta y_{n,k}(j\omega) = y_{n,k}(j\omega) - y_{n,k-1}(j\omega), \quad \forall k \ge 1,$$
 (7)

and

$$I_{y\ell,k}(j\omega) = y_{\ell,k}(j\omega) - y_{\ell,k-1}(j\omega), \tag{8}$$

is the difference of the linear dynamics response part of the output in the  $k^{th}$  iteration (see Eq. (1)).

#### 1) CONVERGENCE ANALYSIS:

Lemma 1: At any given frequency  $\omega$  at which ODDD-IIC is applied, the next-iteration tracking error  $e_{k+1}(j\omega)$   $(k \ge 1)$  (1) satisfies the following recursive formula,

$$e_{k+1}(j\omega) = \mathbb{D}_k(j\omega)e_k(j\omega) - \delta y_{n,k+1}(j\omega), \quad (9)$$

where, respectively,

$$\mathbb{D}_{k}(j\omega) = 1 - \rho_{k}(\omega)\mathbb{G}(j\omega)\frac{I_{u,k}(j\omega)}{I_{u,k}(j\omega)},\tag{10}$$

and  $y_{n,k}(j\omega)$  is the output disturbance in the  $k^{th}$  iteration. (2) is related to the initial tracking error and the disturbance via

$$e_{k+1}(j\omega) = \prod_{i=1}^{k} \mathbb{D}_{k+1-i}(j\omega)e_1(j\omega) - \xi_k(j\omega) - \delta y_{n,k+1}(j\omega),$$
(11)

where

$$\xi_{k}(j\omega) = \begin{cases} 0, & k = 1, \\ \sum_{j=1}^{k-1} (\prod_{i=1}^{j} \mathbb{D}_{k+1-i}(j\omega)) \delta y_{n,k+1-j}(j\omega), & k \ge 2, \end{cases}$$
(12)

*Proof:* The results can be shown via algebraic operation to obtain the recursive formula in Eqs. (9), and then, Eq. (11) by induction.

Next we discuss the convergence of the ODDD-IIC algorithm for the *finite iteration* case, i.e.,  $|\aleph_k(j\omega)| \leq \eta$  for any  $1 \leq k < \mathbf{k}^*$ , and  $|\aleph_k(j\omega)| > \eta$  for  $k \geq \mathbf{k}^*$ . Such a scenario occurs when the ODDD-IIC is convergent and the iterative control input becomes close to each other, i.e.,  $I_{u,k}(j\omega)$  in Eq. (6) becomes small enough to render  $|\aleph_k(j\omega)| > \eta$  when  $k \geq \mathbf{k}^*$ . Thus, we show the convergence by quantifying the upper bound of the relative tracking error given by

$$E_{r,k+1}(j\omega) = \left| \frac{e_{k+1}(j\omega)}{y_d(j\omega)} \right|, \quad \text{for } \forall \ k \ge \mathbf{k}^*, \tag{13}$$

when finite iterations occurs at  $k^*$ .

Theorem 1: For any given frequency  $\omega \in \mathcal{S}_t$  and any  $(k+1)^{th}$  iteration  $(k \geq 1)$ , let the iterative coefficient needed  $\rho_k(j\omega)$  be chosen as:

$$0 < \rho_{min} \le \rho_k(\omega) \le \rho_{max} < 2 + 2Re(\aleph_k(j\omega)), \tag{14}$$

where Re(z) denotes the real part of the complex number  $z \in \mathbb{C}$  ( $\mathbb{C}$ : the set of complex numbers), then when finite iteration stops at any given number  $\mathbf{k}^*$ , the relative tracking error is bounded as

$$E_{r,k+1}(j\omega) \le \left[ \left| \frac{e_1(j\omega)}{y_d(j\omega)} \right| \tau^{\mathbf{k}^*} + \frac{1 - \tau^{\mathbf{k}^*}}{1 - \tau} 2\varepsilon_n \right],$$

$$\triangleq E_{r,1}(j\omega)\tau^{\mathbf{k}^*} + E_{\tau}^{\mathbf{k}^*} \triangleq \mathbf{E}_{r,\tau}^{\mathbf{k}^*},$$
(15)

for any  $k \ge \mathbf{k}^*$ , where

$$E_{\tau}^{\mathbf{k}^*} = \frac{1 - \tau^{\mathbf{k}^*}}{1 - \tau} 2\varepsilon_n, \tag{16}$$

and  $\tau \in [0,1)$  is given by

$$\tau = \sqrt{1 + \max_{1 \le k \le k^*} \left\{ \mathcal{H}[\rho_k(\omega)] \right\}},\tag{17}$$

with  $\mathcal{H}[\rho_k(\omega)]$  defined as

$$\mathcal{H}[\rho_k(\omega)] = \frac{\rho_k(\omega)[\rho_k(\omega) - 2[1 + Re(\aleph_k(j\omega))]]}{(1+\eta)^2}.$$
 (18)

Proof:

By Lemma 1 (Eqs. (9, 10)), the convergence is reached if and only if  $|\mathbb{D}_k(j\omega)| < 1$  for all  $k \ge 1$ , i.e.,

$$|\mathbb{D}_{k}(j\omega)|^{2} = \left|1 - \rho_{k}(\omega) \frac{1}{\frac{I_{y,k}(j\omega)}{\mathbb{G}(j\omega)I_{u,k}(j\omega)}}\right|^{2}$$

$$= \left|\frac{1 + \aleph_{k}(j\omega) - \rho_{k}(\omega)}{1 + \aleph_{k}(j\omega)}\right|^{2}$$

$$= \frac{(1 + |\aleph_{k}(j\omega)| \cos \angle \aleph_{k}(j\omega) - \rho_{k}(\omega))^{2}}{|1 + \aleph_{k}(j\omega)|^{2}} \qquad (19)$$

$$+ \frac{(|\aleph_{k}(j\omega)| \sin \angle \aleph_{k}(j\omega))^{2}}{|1 + \aleph_{k}(j\omega)|^{2}}$$

$$= 1 + \frac{\rho_{k}(\omega)(\rho_{k}(\omega) - 2(1 + Re(\aleph_{k}(j\omega)))}{|1 + \aleph_{k}(j\omega)|^{2}}$$

$$\triangleq 1 + \mathcal{R}(\rho_{k}(\omega), \aleph_{k}(j\omega)) < 1.$$

The above condition holds if  $\rho_k(\omega)$  can be chosen such that

$$-1 < \mathcal{R}(\rho_k(\omega), \aleph_k(j\omega)) < 0, \tag{20}$$

or equivalently,

$$\rho_k(\omega)(\rho_k(\omega) - 2(1 + Re(\aleph_k(j\omega))) < 0, \text{ and} 
|\rho_k(\omega)(\rho_k(\omega) - 2(1 + Re(\aleph_k(j\omega)))| < |1 + \aleph_k(j\omega)|^2.$$
(21)

Solving the above inequality for  $\rho_k(j\omega)$  leads to the range of  $\rho_k(j\omega)$  in Eq. (14) under the condition that  $|\aleph_k(j\omega)| \leq \eta < 1$  for all  $k \geq 1$ .

Thus, if finite iterations occur at  $k^*$ , then there exists a constant  $\tau$  specified by Eqs. (17-18), such that

$$|\mathbb{D}_k(j\omega)|^2 \le \tau^2 < 1 \text{ for } 1 \le k \le \mathbf{k}^*, \tag{22}$$

where  $\tau \in [0,1)$  is guaranteed since  $\mathcal{H}[\rho_k(\omega)] \in [-1,0)$  for all  $1 \leq k \leq \mathbf{k}^*$ . This follows by noting that  $\mathcal{H}[\rho_k(\omega)]$  as a quadratic polynomial of  $\rho$  has its minimal greater than or equaling to -1, and its value is always less than zero for any  $\rho_k(j\omega) \in [\rho_{min}, \rho_{max}]$ .

By Lemma 1 and the triangle inequality, at any  $k \ge \mathbf{k}^*$ , the tracking error can be bounded from Eq. (19), (22) as

$$|e_{k+1}| = \left| \prod_{i=1}^{k} \mathbb{D}_{k+1-i}(j\omega) e_1(j\omega) - \xi_k(j\omega) - \delta y_{n,k+1}(j\omega) \right|$$

$$\leq \left| \prod_{i=1}^{k} \mathbb{D}_{k+1-i}(j\omega) e_1(j\omega) \right| + |\xi_k(j\omega)| + |\delta y_{n,k+1}(j\omega)|.$$
(23)

Then the bound of the relative error in Eq. (15) follows directly by applying Assumption 1 and the summation of a

geometry series to the above Eq. (23). This completes the proof.

Remark 1 (Geometry Interpretation): The convergence condition given by Eq. (19) can be represented by 2-D vector operations as shown in Fig. 2: by Eq. (19) (second "="), for  $\rho_k(\omega) > 0$  the convergence is guaranteed if the length of vector  $\overrightarrow{OA} = |1 + \aleph_k(\omega) - \rho_k(\omega)|$  is less than that of vector  $\overrightarrow{OB} = |1 + \aleph_k(\omega)|$ , i.e., the vector  $\overrightarrow{OA}$  falls into the triangle of FOB specified by  $\overrightarrow{OB}$  and its y-axis symmetry  $\overrightarrow{OF}$ . Thus, the length of  $|\overrightarrow{BF}| = 2 + 2Re(\aleph_k(j\omega))$  is the range of  $\rho_k(\omega) > 0$  that guarantees the convergence—exactly the same as given by Eq. (14).

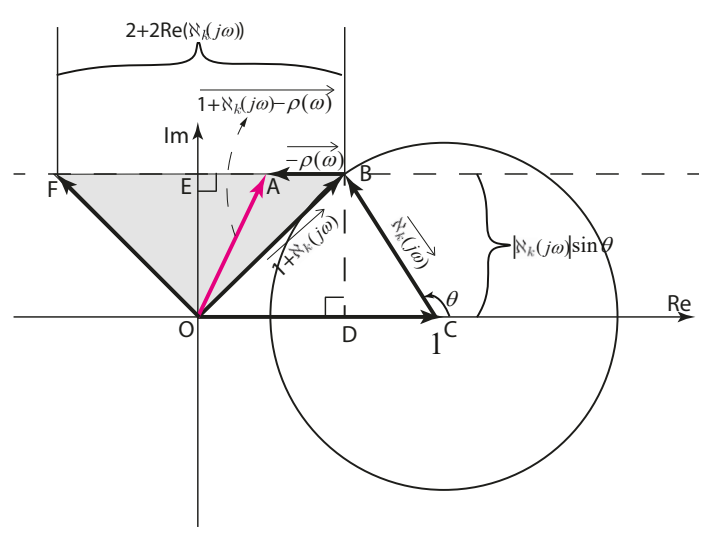


Fig. 2. The geometry interpretation of Theorem 1 and Corollary 1, where the symbols denote the vectors represented by the corresponding arrowed lines, and  $\overrightarrow{OF}$  denotes the y-axis symmetric vector of  $\overrightarrow{OB}$ , i.e.,  $|\overrightarrow{OF}| = |\overrightarrow{OB}| = |\overrightarrow{1+\aleph_k}|$ .

Theorem 1 shows the residual error (i.e., the radius of the neighborhood) depends on the range of the iterative coefficients  $\rho_k(j\omega)$ s used in the iterations (i.e., the maximum and the minimum of  $\rho_k(j\omega)$ , see Eq. (14)). In particular, when a *fixed* iterative coefficient is chosen in all the iterations, the residual error agrees with that quantified in [11].

Alternatively, an optimal iterative coefficients can be sought to minimize the residual error, as shown below. The convergence range of the iterative coefficient varies along with the iterations (see Eq. (14)): In general, the variation is small initially (so  $\rho_k(j\omega)$  can be chosen in an interval closely around (0, 2)) then increases with the iterations (k is large).

#### 2) Estimation of the Noise to Output Difference Ratio:

Next we discuss how to estimate the NODR  $|\aleph_k(j\omega)|$  in practice—as needed in determining the range of the iteration gain  $\rho_k(j\omega)$  (see Eq. (14)). As the exact dynamics,  $\mathbb{G}(j\omega)$ , in general, is unknown, uncertainty in the dynamics modeling shall be accounted for when quantifying the NODR. Thus, we first represent the NODR,  $|\aleph_k(j\omega)|$ , using measured frequency

response as

$$|\aleph_{k}(j\omega)| = \left| \frac{\hat{\mathbb{G}}(j\omega)}{\mathbb{G}(j\omega)} \frac{\delta y_{n,k}(j\omega)}{\hat{\mathbb{G}}(j\omega)I_{u,k}(j\omega)} \right| \triangleq \left| \Delta \mathbb{G}(j\omega)\hat{\aleph}_{k}(j\omega) \right|$$
$$= \left| \Delta \mathbb{G}(j\omega) \left( \frac{I_{y,k}(j\omega)}{\hat{\mathbb{G}}(j\omega)I_{u,k}(j\omega)} - 1 \right) \right| \leq \eta < 1,$$
(24)

where  $\hat{\mathbb{G}}(j\omega)$  denotes the measured frequency response— $\Delta\mathbb{G}$  is the relative difference between the measured and the true frequency response of the system, and  $\hat{\aleph}_k(j\omega)$  is the estimated NODR, respectively.  $\Delta\mathbb{G}(j\omega)$ , although still unknown in general, can be estimated by the upper/lower bounds of the differences between the frequency responses measured under different conditions [26], i.e.,

$$\Delta \mathbb{G}(j\omega) = \Delta r(\omega) \cdot e^{j\Delta\theta(\omega)}, \text{ with} 
0 < \Delta r_{\min}(\omega) \le \Delta r(\omega) \le \Delta r_{\max}(\omega), 
\Delta \theta_{\min}(\omega) \le \Delta \theta(\omega) \le \Delta \theta_{\max}(\omega),$$
(25)

where, respectively,

$$\Delta r_{\max}(\omega) = \max_{i,j} \left| \frac{\hat{\mathbb{G}}_i(j\omega)}{\hat{\mathbb{G}}_j(j\omega)} \right|,$$

$$\Delta \theta_{\max}(j\omega) = \max_{i,j} \left\{ \angle \hat{\mathbb{G}}_i(j\omega) - \angle \hat{\mathbb{G}}_j(j\omega) \right\},$$
(26)

 $\hat{\mathbb{G}}_i(j\omega)(i=1,2,\cdots)$  denotes the  $i^{th}$  frequency response measured in the experiment, and  $\Delta r_{\min}(\omega)$  and  $\Delta \theta_{\min}(j\omega)$  are defined similarly. Hence, the magnitude and phase of the NODR can be bounded as

$$\Delta r_{\min}(\omega)|\hat{\aleph}_k(j\omega)| \le |\aleph_k(j\omega)| \le \Delta r_{\max}(\omega)|\hat{\aleph}_k(j\omega)|,$$
 (27)

and

$$\angle \hat{\aleph}_k(j\omega) + \Delta\theta_{\min}(\omega) \le \angle \aleph_k(j\omega)$$

$$\le \angle \hat{\aleph}_k(j\omega) + \Delta\theta_{\max}(\omega).$$
(28)

Thus, NODR can be quantified in terms of the measured dynamics difference and the measured NODR  $\hat{\aleph}_k(j\omega)$ —by using the measured frequency responses (see Eqs. (25), (26)) along with the measured input-output data in each iteration,  $I_{y,k}(j\omega)$  and  $I_{u,k}(j\omega)$ . Using the estimated NODR, the convergence of the ODDD-IIC algorithm can be presented for practical implementation via the following Corollary.

Corollary 1: At any given frequency  $\omega$ , let the conditions in Theorem 1 be hold, and the measured phase difference of the system dynamics be less than  $\pi/2$ ,

$$0 \le |\Delta \theta_{\max}(j\omega) - \Delta \theta_{\min}(j\omega)| < \frac{\pi}{2}, \tag{29}$$

then the ODDD-IIC law converges if in each  $(k+1)^{th}$  iteration  $(k=1, 2, \cdots)$ , the iterative coefficient  $\rho_k(\omega)$  is chosen from

$$0 < \rho_k(\omega) < 2 + 2\nu_k^*,\tag{30}$$

where

$$\nu_{k}^{\perp} = \begin{cases} |\aleph_{k}^{\perp}(j\omega)| \cos \angle \aleph_{k}^{\top}(j\omega), \\ \text{if } \angle \aleph_{k}^{\perp}(j\omega), \angle \aleph_{k}^{\top}(j\omega) \in (0, \frac{\pi}{2}]; \\ |\aleph_{k}^{\top}(j\omega)| \cos \angle \aleph_{k}^{\top}(j\omega), \\ \text{if } \angle \aleph_{k}^{\top}(j\omega) \in (\frac{\pi}{2}, \pi); \\ - |\aleph_{k}^{\top}(j\omega)|, \\ \text{if } \angle \aleph_{k}^{\perp}(j\omega) \in (\frac{\pi}{2}, \pi), \angle \aleph_{k}^{\top}(j\omega) \in [\pi, \frac{3\pi}{2}); \\ |\aleph_{k}^{\top}(j\omega)| \cos \angle \aleph_{k}^{\perp}(j\omega), \\ \text{if } \angle \aleph_{k}^{\perp}(j\omega) \in (\pi, \frac{3\pi}{2}]; \\ |\aleph_{k}^{\perp}(j\omega)| \cos \angle \aleph_{k}^{\perp}(j\omega), \\ \text{if } \angle \aleph_{k}^{\perp}(j\omega), \angle \aleph_{k}^{\top}(j\omega) \in (\frac{3\pi}{2}, 2\pi]; \\ |\aleph_{k}^{\perp}(j\omega)| \min\{\cos \angle \aleph_{k}^{\perp}(j\omega), \cos \angle \aleph_{k}^{\top}(j\omega)\}, \\ \text{if } \angle \aleph_{k}^{\perp}(j\omega) \in (\frac{3\pi}{2}, 2\pi], \angle \aleph_{k}^{\top}(j\omega) \in (2\pi, \frac{5\pi}{2}]. \end{cases}$$

$$(31)$$

where, respectively,  $|\aleph_k^{\top}(j\omega)|$ ,  $|\aleph_k^{\perp}(j\omega)|$ ,  $\angle \aleph_k^{\top}(j\omega)$ , and  $\angle \aleph_k^{\perp}(j\omega)$  are given by

$$|\aleph_{k}^{\top}(j\omega)| = \Delta r_{\max}(\omega)|\hat{\aleph}_{k}(j\omega)|$$

$$|\aleph_{k}^{\perp}(j\omega)| = \Delta r_{\min}(\omega)|\hat{\aleph}_{k}(j\omega)|$$

$$\angle \aleph_{k}^{\perp}(j\omega) = \angle \hat{\aleph}_{k}(j\omega) + \Delta \theta_{\min}(\omega)$$

$$\angle \aleph_{k}^{\top}(j\omega) = \angle \hat{\aleph}_{k}(j\omega) + \Delta \theta_{\max}(\omega)$$
(32)

*Proof:* The proof is similar to that of Theorem 1, by replacing NODR  $|\aleph_k(j\omega)|$  with its bounds in amplitude and phase as given by Eq. (24), (27) and (28), respectively. Then the range of the iterative coefficient  $\rho_k(\omega)$  for convergence can be represented by the bounds of NODR, as given in Eqs. (30) and (31), respectively.

Remark 2: The upper bound of the iterative coefficient  $\rho_k(j\omega)$  is well defined, as before every  $k^{th}$  iteration, all the terms in the bound are already known, and thereby can be used to quantify the value of  $\rho_k(j\omega)$  used in the next  $k^{th}$  iteration.

3) OPTIMAL ITERATION GAIN:

Theorem 2: At any given frequency  $\omega$ , let the conditions in Corollary 1 be satisfied, then with the following choice of the iterative gain,  $\rho_k^*(\omega)$ ,

$$\rho_k^*(\omega) = 1 + |\aleph_k(j\omega)| \cos \angle \aleph_k(j\omega), \tag{33}$$

- (1) the convergence rate is maximized, i.e., for any  $k \geq 2$ ,  $|\mathbb{D}_k(j\omega)|$  is maximum at  $\rho_k(\omega) = \rho_k^*(\omega)$ .
- (2) the upper bound of the residual tacking error is minimized, i.e.,

$$E_{r,k}(j\omega) \triangleq \mathbf{E}_{r,n}^{\mathbf{k}^*} < \mathbf{E}_{r,\tau}^{\mathbf{k}^*}, \tag{34}$$

where  $\mathbf{E}_{r,\eta}^{\mathbf{k}^*}$  has the same expression as  $\mathbf{E}_{r,\tau}^{\mathbf{k}^*}$  given in Eq. (15) with  $\tau$  replaced by  $\eta$ , and

$$E_{\eta}^{\mathbf{k}^*} = \frac{1 - \eta^{\mathbf{k}^*}}{1 - \eta} 2\varepsilon_n < E_{\tau}^{\mathbf{k}^*}, \tag{35}$$

(3) the use of the ODDD-IIC consistently improves the tracking at frequency  $\omega$ , i.e.,

$$E_{r,k}(j\omega) < 1$$
, for  $2 \le k \le \mathbf{k}^*$ , (36)

if for any given NSR less than 0.5, i.e.,  $\varepsilon_n <$  0.5, the NODR is bounded above by  $\eta < \eta^* < 1$  with

$$\eta^* = \frac{1}{2E_{r,1}(j\omega)} \left[ E_{r,1}(j\omega) + 1 - \sqrt{\hat{E}_{r,1}(j\omega)} \right],$$

$$\hat{E}_{r,1}(j\omega) \triangleq (E_{r,1}(j\omega) + 1)^2 - 4E_{r,1}(j\omega)(1 - 2\varepsilon_n). \tag{37}$$

*Proof:* By Eq. (23), the value of  $\rho_k(\omega)$  that minimizes the upper bound of  $|\mathbb{D}_k(\rho_k(\omega))|$  minimizes and maximizes the upper bound of the residual error and the convergence rate, respectively. Being quadratic in  $\rho_k(\omega)$ ,  $|\mathbb{D}_k(\rho_k(\omega))|^2$  is minimized when  $\rho_k(\omega)$  is chosen as in Eq. (33), i.e., at  $\rho_k(\omega) = \rho_k^*(\omega)$ ,

$$|\mathbb{D}_{k}^{*}(j\omega)|^{2} = \left| \frac{1 + \aleph_{k}(j\omega) - 1 - |\aleph_{k}(j\omega)| \cos \angle \aleph_{k}(j\omega)}{1 + \aleph_{k}(j\omega)} \right|^{2}$$

$$= \frac{(|\aleph_{k}(j\omega)| \sin \angle \aleph_{k}(j\omega))^{2}}{|1 + \aleph_{k}(j\omega)|^{2}}$$

$$< |\mathbb{D}_{k}(j\omega)|^{2}, \quad (\text{for } \rho_{k}(\omega) \neq \rho_{k}^{*}(\omega))$$
(38)

therefore

$$\sup_{\aleph_k} |\mathbb{D}_k^*(j\omega)| = \eta < \sup_{\aleph_k} |\mathbb{D}_k(j\omega)| = \tau < 1.$$
 (39)

And by lemma 1 (Eqs. (9-11)) and the triangle inequality, the relative error is also minimized by setting  $\rho_k(\omega) = \rho_k^*(\omega)$  the relative error is also minimized as given in Eq. (34).

Finally, to find the upper bound of NODR,  $\eta$ , for improving the tracking consistently, we note that with the optimal iterative gain  $\rho_k^*(\omega)$ , by Eq. (34),

$$E_{r,k}(j\omega) < \left[ E_{r,1}(j\omega)\eta + \frac{1}{1-\eta} 2\varepsilon_n \right] < 1, \tag{40}$$

for  $\forall k \geq \mathbf{k}^*$ . Solving the above inequality for the upper bound of  $\eta$  leads to  $\eta^*$  given in Eq. (37), and it can be verified that for  $\varepsilon_n \in (0, 1/2), \ \eta^* < 1$ . This completes the proof.

Remark 3 (Geometry Interpretation): As shown in Fig. 2, the length of the vector  $\overrightarrow{OA}$  equals to its minima,  $\overrightarrow{OE}$ , when  $\rho_k(\omega)=1+Re(\aleph_k)$ , so is  $|\mathbb{D}_k(j\omega)|=|\mathbb{D}_k^*(j\omega)|=|\overrightarrow{OE}|/|\overrightarrow{OB}|$ , and the convergence rate is maximized. Meanwhile, the upper bound of the residual error is inversely proportional to the upper bound of  $|\mathbb{D}_k(j\omega)|$  (see Eq. (23)). Therefore, when  $\rho_k(\omega)=1+Re(\aleph_k)$ , both minimal upper bound of the residual error and maximal convergence rate are reached simultaneously.

Remark 4: In practice, the optimal iteration gain  $\rho_k^*(\omega)$  can be approximated by using an estimated NODR. For example, the NODR can be estimated by using the averaged value of the frequency responses obtained in multiple measurements to replace the true value of the frequency response in Eq. (24), and the estimated NODR is then used to compute the optimal gain via Eq. (33).

Remark 5: For guaranteed consistent tracking improvement, the allowed NSR  $\varepsilon_n < 1/2$  is larger than that for the modeling-free inversion-based iterative control (MIIC) at  $(1-\sqrt{2}/2) \approx 0.3$  [11]. Also, the allowable NODR  $\eta^*$  quantified above is quite large. For example, when  $\varepsilon_n < 3/16$  and  $E_{r,1}(j\omega) < 1/2$ , as large as  $\eta^* = 1/2$  is allowed.

### B. ROBUSTNESS AND PERFORMANCE IMPROVEMENT OVER MFDIIC

Next, we discuss the improvement of the proposed ODDD-IIC over the previously proposed constant-gain MFDIIC algorithm [10] in both performance and robustness, where

$$u_{k+1}(j\omega) = u_k(j\omega) + \rho \frac{I_{u,k}(j\omega)}{I_{y,k}(j\omega)} \times e_k(j\omega), \ k \ge 1, \quad (41)$$

where  $u_0(j\omega)$  and  $u_1(j\omega)$  are the same as given in Eq. (3) respectively. First, we can show similarly as Theorem 1 the convergence of MFDIIC as stated below

Theorem 3: At any frequency  $\omega$ , let the NODR be less than 1/2, i.e.,

$$|\aleph_k(j\omega)| = \left| \frac{I_{y,k}(j\omega)}{\mathbb{G}I_{u,k}(j\omega)} - 1 \right| \le \eta_M < \frac{1}{2}, \qquad k \ge 1, \quad (42)$$

then with  $\rho=1$ , the MFDIIC converges and the relative tracking error is bounded as

$$E_{r,k+1} \le \left(\frac{\eta_M}{1 - \eta_M}\right)^{k^*} E_{r,1} + \frac{2 - 2\eta_M}{1 - 2\eta_M} \varepsilon_n$$
 (43)

for any  $k > k^*$ .

The proof is similar to Theorem 1 and is omitted. The above Theorem 3 shows that the proposed ODDD-IIC, by employing a frequency and iteration dependent coefficient  $\rho_k(\omega)$ , allows a larger NODR than the constant-coefficient MFDIIC does, resulting in an improvement in both robustness and performance (from a larger frequency range of convergence). More specifically, we have the following Theorem.

Theorem 4: Let the conditions in Theorem 1 be satisfied at frequency  $\omega$ , then

(1) By choosing the iteration gain  $\rho_k(\omega)$  as

$$\begin{cases} 1 - 2|\aleph_k^\top(j\omega)| < \rho_k(\omega) < 1, & \text{if } \angle \aleph_k(j\omega) \in (\frac{\pi}{2}, \frac{3\pi}{2}), \\ \text{or} \\ 1 \le \rho_k(\omega) < 1 + 2|\aleph_k^\perp(j\omega)|, & \text{otherwise}, \end{cases}$$

$$\tag{44}$$

the ODDD-IIC converges faster than or at least not slower than that of MFDIIC, i.e.,

$$|\mathbb{D}_k(j\omega)| \le |\mathbb{E}_k(j\omega)| < 1,\tag{45}$$

where  $\mathbb{D}_k(j\omega)$  is as in Eq. (10), and  $\mathbb{E}_k(j\omega)$  given by

$$\mathbb{E}_k(j\omega) = 1 - \mathbb{G}(j\omega) \frac{I_{u,k}(j\omega)}{I_{y,k}(j\omega)}, \qquad k \ge 1,$$
 (46)

is as  $\mathbb{D}_k(j\omega)$  in Eq. (9) when the ODDD-IIC is replaced with the MFDIIC law.

(2) For frequencies  $\omega_d \in \mathcal{S}_k$ , where

$$S_k = \left\{ \omega_d \middle| |\aleph_k(\omega_d)| \in (\frac{1}{2}, 1) \right\},\tag{47}$$

the convergence of the ODDD-IIC algorithm is guaranteed by choosing  $\rho_k(\omega_d)$  as

$$0 < \rho_k(\omega_d) < 2 - 2|\aleph_k^\top(j\omega_d)|,\tag{48}$$

whereas the convergence of MFDIIC is not guaranteed.

*Proof*: By algebraic operation, it can be verified that showing the ODDD-IIC converges faster than that MFDIIC amounts to showing that

$$\left| 1 - \rho_k(\omega) \mathbb{G} \frac{I_{u,k}(j\omega)}{I_{y,k}(j\omega)} \right| \le \left| 1 - \mathbb{G} \frac{I_{u,k}(j\omega)}{I_{y,k}(j\omega)} \right|. \tag{49}$$

Or equivalently,

$$[\rho_k(\omega) - (1 + |\aleph_k|\cos\angle\aleph_k(j\omega))]^2 \le |\aleph_k|^2\cos^2\angle\aleph_k(j\omega).$$
(50)

By considering the sign of  $\cos \angle \aleph_k(j\omega)$ , it can be verified that the above inequality (50) holds by choosing  $\rho_k(\omega)$  as in Eq. (44).

To show Statement 2, it can be verified that for  $\omega_d \in \mathcal{S}_k$ , by choosing  $\rho_k(\omega_d)$  as in Eq. (48) we have  $|\mathbb{D}_k(j\omega_d)| < 1$ , and thereby, ODDD-IIC converges. However, for  $\omega_d \in \mathcal{S}_k$ , when the phase of NODR,  $\angle \aleph_k(j\omega_d)$ , falls into the range of

$$\pi - \arccos(\frac{1}{2|\aleph_k^{\perp}(j\omega_d)|}) < \angle \aleph_k(\omega_d)$$

$$< \pi + \arccos(\frac{1}{2|\aleph_k^{\perp}(j\omega_d)|}),$$
(51)

we have

$$1 + 2|\aleph_k(j\omega_d)|\cos \angle \aleph_k(j\omega_d) < 0.$$
 (52)

Or, equivalently

$$\left| \frac{\aleph_k(j\omega_d)}{1 + \aleph_k(j\omega_d)} \right| > 1, \tag{53}$$

and thereby

$$|\mathbb{E}_{k}(j\omega_{d})| = \left|1 - \mathbb{G}\frac{I_{u,k}(j\omega_{d})}{I_{y,k}(j\omega_{d})}\right|$$

$$= \left|1 - \frac{1}{1 + \aleph_{k}(j\omega_{d})}\right| > 1.$$
(54)

The disturbance,  $\delta y_{n,k}(j\omega_d)$ , being random implies that the NODR,  $\aleph_k(j\omega_d)$ , is also random in each iteration. Thus, there exist iterations during which Eq. (50) holds, and thereby  $|\mathbb{E}_k(j\omega_d)| > 1$ . The randomness nature of NODR also implies that  $|\mathbb{E}_k(j\omega_d)| > 1$  occurs during the entire process, and no asymptotic convergence can be guaranteed. This completes the proof.

Remark 6: The condition of Eq. (44) is well-defined: Although the NODR,  $\aleph_k(j\omega)$ , is random, after each iteration its angle and phase in that iteration are determined and known, thereby, can be used to check and design  $\rho_k(\omega)$ . In practice, the phase condition of  $\angle \aleph_k(j\omega)$  can be estimated by using  $\angle \hat{\aleph}_k(j\omega)$  as in Corollary 1. Therefore, Theorem 4 characterizes the improvements the proposed ODDD-IIC over

the constant-gain MFDIIC algorithm in both performance and robustness.

As a summary, we describe the implementation of the proposed ODDD-IIC algorithm in the following Algorithm.

#### Algorithm 1: Implementation of the ODDD-IIC

- 1 Measure the noise level of the system,  $y_n(j\omega)$ , and the frequency responses of the system,  $\hat{\mathbb{G}}(j\omega)$ , under different conditions.
- 2 Estimate the range of magnitude and phase variations by Eqs. (25), (26).
- **3** Estimate the NSR via Eqs. (2) and determine the frequency range within which the algorithm is applied.
- 4 Obtain an initial input  $u_0(j\omega)$  by choosing a constant  $\alpha$  in Eq. (1) (e.g. DC gain of the system).
- 5 Apply  $u_0(j\omega)$  to the system, acquire the output  $y_0(j\omega)$ .
- 6 Substitute  $u_0(j\omega)$  and  $y_0(j\omega)$  into Eq. (2) to obtain  $u_1(j\omega)$ . if iteration numbers  $k \ge 1$  then
  - (1) Apply  $u_k(j\omega)$  to the system and acquire  $y_k(j\omega)$ ,  $e_k(j\omega)$ .
  - (2) Estimate the NODR  $\aleph_k(j\omega)$  by Eq. (24), and use it determine  $\rho_k^*(j\omega)$  via Eq. (33).
  - (3) Determine  $u_{k+1}(j\omega)$  using Eq. (5) from  $u_k(j\omega)$ ,  $u_{k-1}(j\omega)$ ,  $y_{k-1}(j\omega)$ ,  $y_k(j\omega)$  and  $\rho_k(j\omega)$ .
  - (4) Set  $k \leftarrow k+1$ , repeat from (1) to (3) until the convergence is reached.

#### III. EXPERIMENTAL EXAMPLE

In this section, we implemented the ODDD-IIC method in output tracking of a piezoelectric actuator.

#### A. EXPERIMENTAL SETUP

The piezoactuator was employed for the positioning and actuation in an atomic force microscope (AFM) system (Dimension ICON, Bruker-Nano Inc.). All control algorithms and inputs were coded and generated in the MATLAB XPC-target environment (Mathworks Inc.). The PID controller of the AFM system had been bypassed when external control inputs were applied. The sampling rate was set at 40 KHz. Triangle signals at four different rates (100 Hz, 200 Hz, 320 Hz, and 400 Hz) and the following multi-sine wave signal,  $y_{d,ms}(t)$ , were chosen as the desired trajectories,

$$y_{d,ms}(t) = \sum_{k=1}^{35} a_k \sin(\omega_k t),$$
 (55)

with  $a_k \in (0,1)$ ,  $\omega_1 = 13$ ,  $\omega_2 = 38$ , and  $\omega_k = 38 + 30(k-2)$  for  $3 \le k \le 35$ , respectively. The hysteresis effect was suppressed by keeping the amplitude of the desired signals less than 9% of the total displacement range of the piezo-actuator.

#### B. IMPLEMENTATION OF THE ODDD-IIC TECHNIQUE

We started the implementation by quantifying the modeling uncertainty of the system,  $\Delta r_{max}(\omega)$  and  $\Delta r_{min}(\omega)$ , to determine the range of the iterative gain  $\rho_k(j\omega)$  (see Eq. (30)). The modeling uncertainty was estimated by measuring the frequency responses (FR) with a band-limited white-noise input at ten different amplitudes. The maximum, minimum, and averaged values of the measured magnitudes and phases are shown in Fig. 2, and the upper and lower bound of the magnitude and the phase differences, are shown in Fig. 4, respectively. The resonance of and the open-loop bandwidth of the system were at 780 Hz and 1.39 KHz, respectively, and the relative magnitude and phase variation around the resonance was at 11.2% and 280%, respectively.

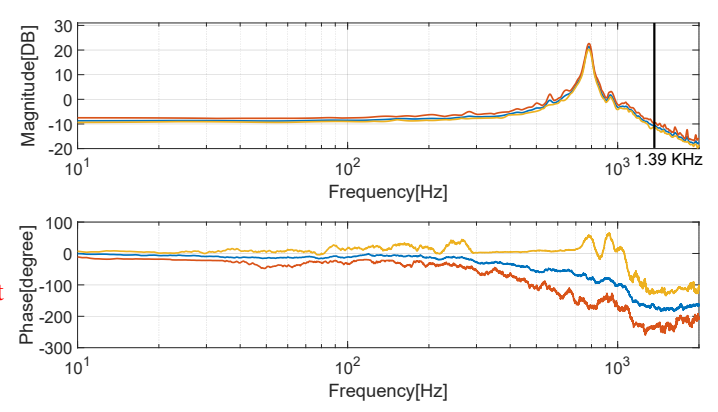


Fig. 3. The averaged measured frequency response (——), the upper bound (——) and the lower bound (——), respectively.

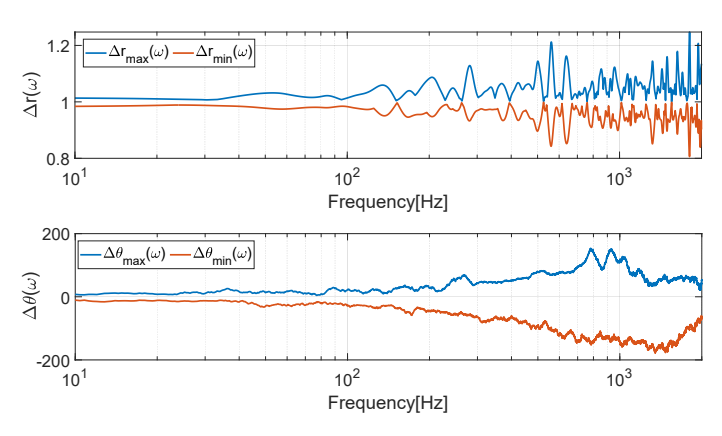


Fig. 4. The upper and lower bound of the magnitude uncertainty  $(\Delta r_{\max}(\omega))$  and  $\Delta r_{\min}(\omega)$ , respectively) and phase uncertainty  $(\Delta \theta_{max}(\omega))$  and  $\theta_{\min}(\omega)$ , respectively).

The implementation was shown in Algorithm 1, which shows that only the frequency response need to be measured a priori, the optimal iteration gain given by Eq. (33) was updated in each iteration at frequencies where the convergence conditions in Eqs. (2), (6) held, and set to zero otherwise. For comparison, the MFDIIC [10] and the IIC [12] were also implemented. A unit iterative coefficient was chosen  $(\rho_k(\omega) = 1 \quad \forall k)$  in the MFDIIC and IIC, and the inverse of the averaged frequency response was used in the IIC algorithm [12]. Moreover, to examine the improvement of the proposed

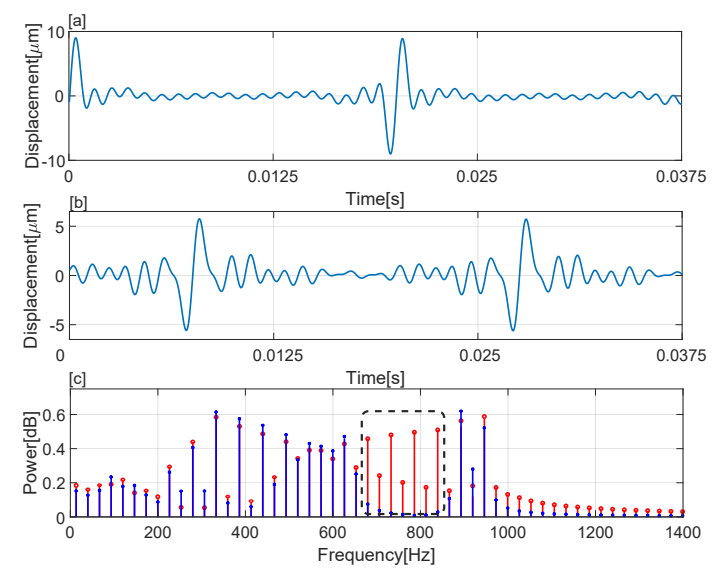


Fig. 5. [a]: the multi-sine wave, [b]: the filtered multi-sine wave trajectory, and [c]: comparison of the power spectrum of the multi-sine wave (—) and and the filtered multi-sine wave (—), respectively, where the frequencies in the dashed box appeared only in the original multi-sine wave.

ODDD-IIC over the constant-gain MFDIIC algorithm (see Theorem 4), the multi-sinewave signal was passed through a fourth-order Butterworth bandpass filter to remove the eight frequency components around the resonant peak of the system at which the convergence condition for the MFDIIC did not hold: 638 Hz, 668 Hz, 698 Hz, 728 Hz, 758 Hz, 788 Hz, 818 Hz and 848 Hz. The original and the filtered multisine waves and their power spectrum are compared in Fig. 5. The filtered signal was tracked by using both the ODDD-IIC and the MFDIIC. In this experiment, the iterations of all the ODDD-IIC/MFDIIC/IIC were terminated when the relative two-norm output error  $E_2(\%)$  and the relative maximum tracking error  $E_{max}(\%)$  could not be further reduced, where  $E_2(\%)$  and  $E_{max}(\%)$  are defined below, respectively,

$$E_2(\%) = \frac{\parallel y_d(\cdot) - y(\cdot) \parallel_2}{\parallel y_d(\cdot) \parallel_2} \times 100\%, \tag{56}$$

$$E_{max}(\%) = \frac{\| y_d(\cdot) - y(\cdot) \|_{\infty}}{\| y_d(\cdot) \|_{\infty}} \times 100\%.$$
 (57)

#### IV. TRACKING RESULTS AND DISCUSSION

#### A. TRACKING RESULTS

The tracking results of the triangle trajectories at four different rates obtained by using the three methods are compared in Fig. 6 and Fig. 7, with the corresponding tracking errors compared in Fig. 8, respectively. The overall relative two-norm,  $E_2(\%)$ , and maximum tacking errors,  $E_{max}(\%)$ , are presented in Fig. 9, and the convergence of  $E_2(\%)$  and  $E_{max}(\%)$  along with the iterations are shown in Fig. 10 for the 400 Hz triangle tracking, respectively.

The output tracking and the tracking error of the original and the filtered multi-sine wave trajectories obtained by using the ODDD-IIC and the MFDIIC technique are shown in Fig. 11

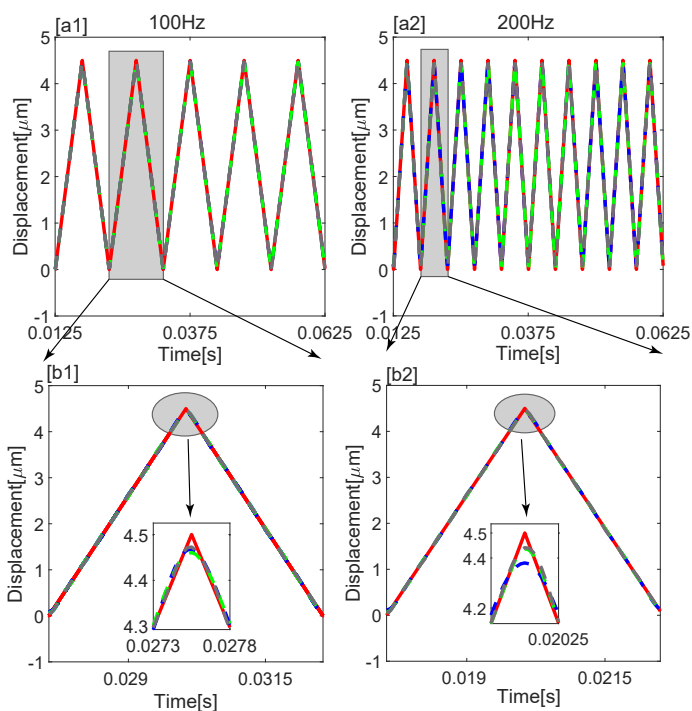


Fig. 6. Comparison of the tracking results of the triangle signal at 100 Hz (a1), and 200 Hz (a2) by using the ODDD-IIC (—), the MFDIIC (—), and the IIC (—) with respect to the reference signal (—), and (b1, b2) are the zoomed-in view of one period in (a1) and (a2), respectively.

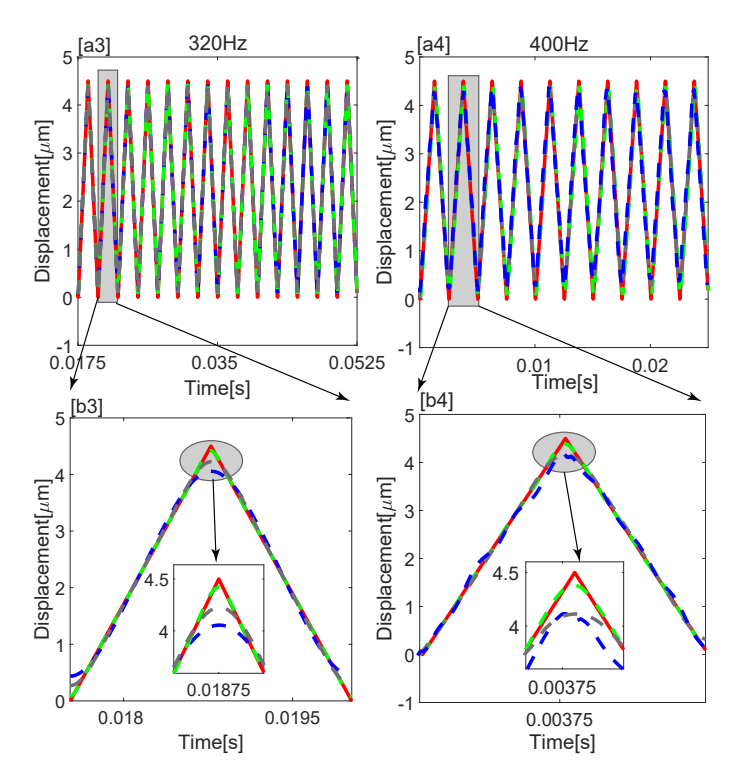


Fig. 7. Comparison of the tracking results of the triangle signal at 320 Hz (a1), and 400 Hz (a2) by using the ODDD-IIC(—), the MFDIIC (—), and the IIC (—) with respect to the reference signal(—), and (b1, b2) are the zoomed-in of one period in (a1) and (a2), respectively.

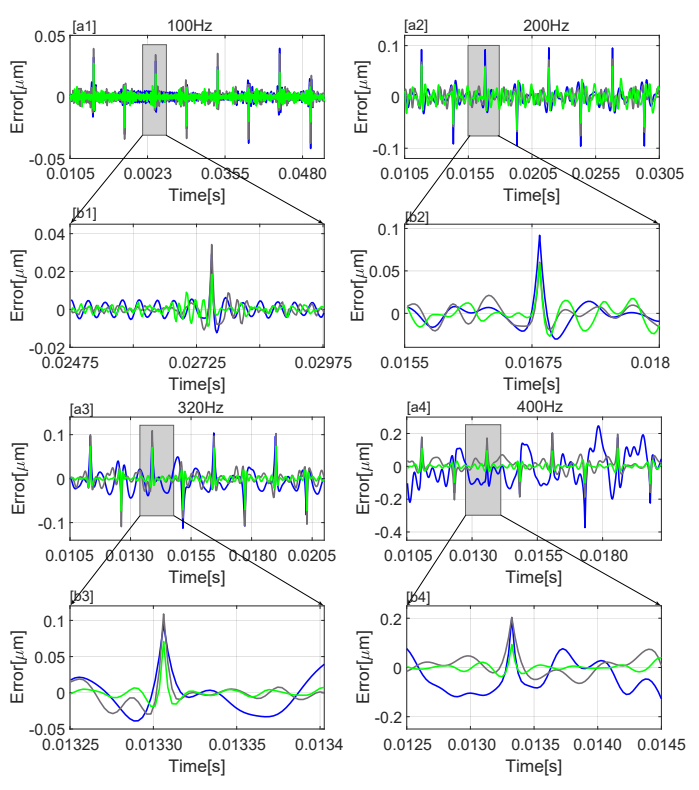


Fig. 8. Comparison of tracking error of the ODDD-IIC (—), MFDIIC (—), and IIC (—) at (a1) 100 Hz, (a2) 200 Hz, (a3) 320 Hz and (a4) 400 Hz, respectively, and (b1), (b2), (b3) and (b4) the zoomed-in view of the gray rectangle area in (a1), (a2), (a3) and (a4), respectively.

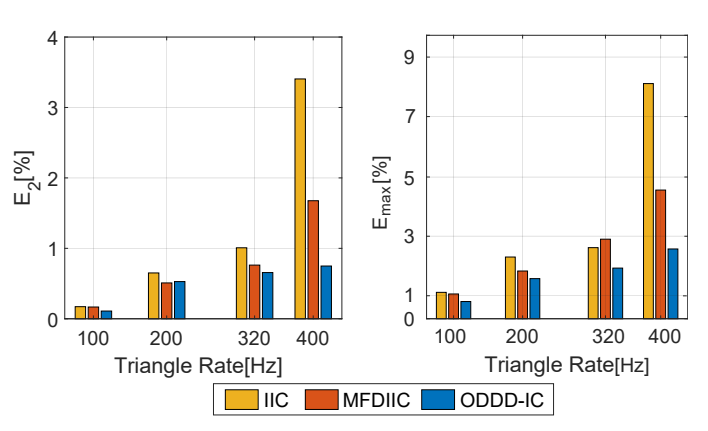


Fig. 9. Comparison of the relative tracking error of IIC, MFDIIC, ODDD-IIC in (left) 2-norm and (right) infinity-norm for the four different triangle rates, respectively.

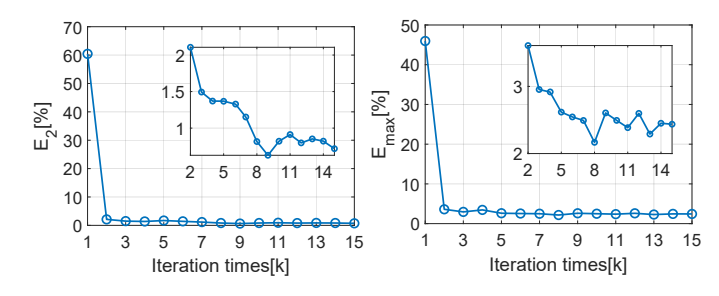


Fig. 10. (left) Relative 2-norm error  $E_2[\%]$  and (right) relative maximum error  $E_{max}[\%]$  of the output tracking for the 400 Hz triangle trajectory by using the ODDD-IIC algorithm in 15 iterations, respectively, where the inserts show the zoomed-in view of the error for the  $2^{dn}$  to  $15^{th}$  iterations, respectively.

(a1) to (b2), respectively. The tracking error is analyzed and compared in Fig. 12 and 13, respectively.

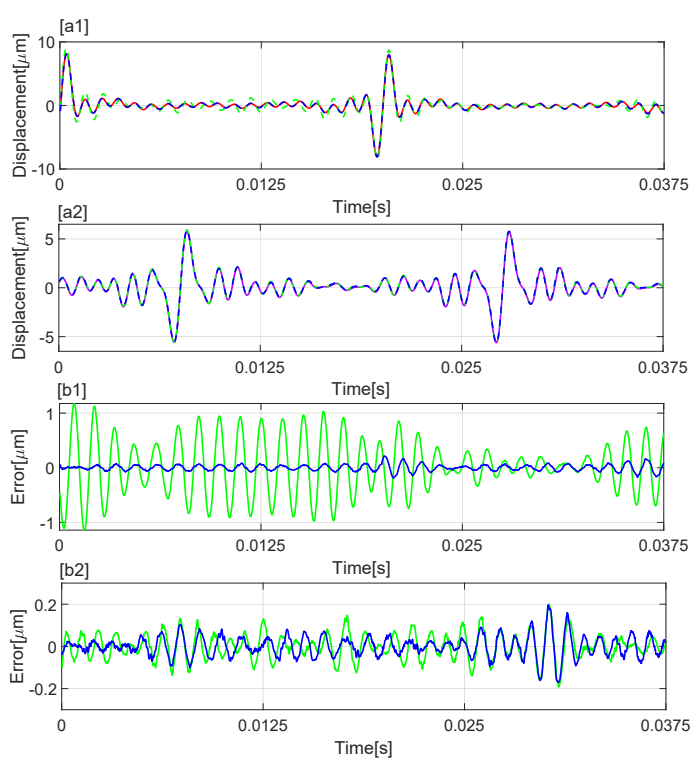


Fig. 11. (a1), (a2): The results of tracking multi-sine wave(—) and filtered multi-sine wave(—) by using ODDD-IIC (—) and MFDIIC (—), respectively. (b1), (b2): The comparison of tracking error by using ODDD-IIC(—) and MFDIIC(—), respectively.

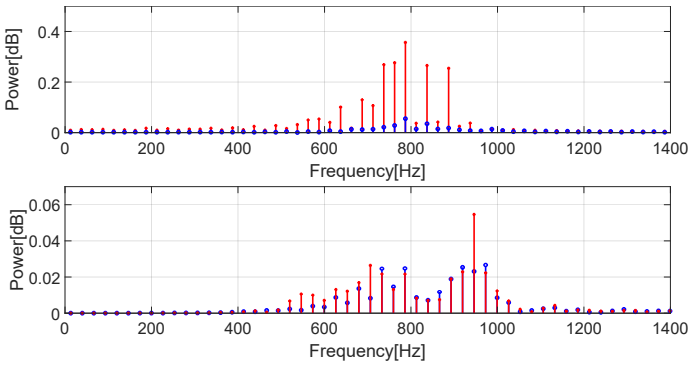


Fig. 12. (top) The power spectrum of the tracking error in tracking multi-sine signal and (bottom) the filtered multi-sine signal by using the ODDD-IIC (—) and the MFDIIC (—), respectively.

#### B. DISCUSSION

1) TRIANGLE TRAJECTORY TRACKING: The experimental results showed that by using the proposed ODDD-IIC technique, the tracking performance can be further improved over the MFDIIC and the IIC techniques—two highly efficient ILC techniques already demonstrated in various applications [10], [26], [27]. At the relatively low triangle rate of 100 Hz, precision tracking was achieved by all the three methods, with the tracking error (in both the relative 2-norm and maximum

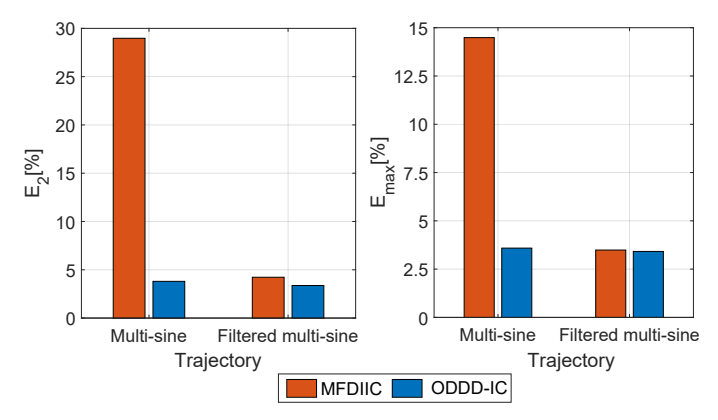


Fig. 13. Comparison of (left) the relieve 2-norm and (right) the relative maximum tracking error of the MFDIIC and the ODDD-IIC when tracking the original and the filtered multi-sine wave tracking results, respectively.

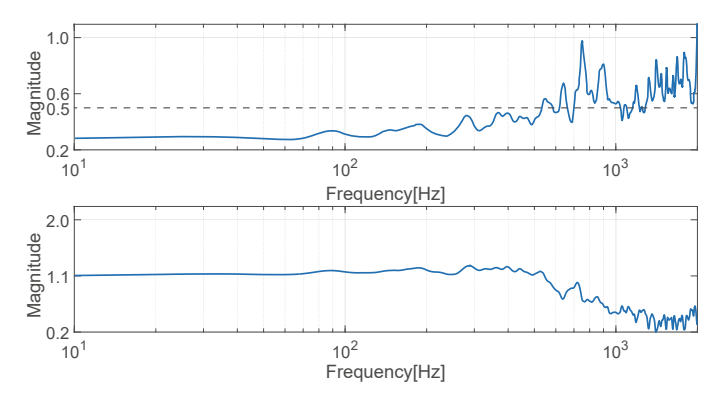


Fig. 14.  $|\hat{\aleph}_5(j\omega)|$  (top) and  $\rho_5(\omega)$  (bottom) when tracking the original multi sine wave. The value of 0.5 ( - ) is plotted in the top figure.

error) all below 1% and 1.5%, respectively (see Fig. 6 (a1), (b1), Fig. 8 (a1), and Fig. 9). Such a precision tracking was maintained when the triangle rate was increased to 200 Hz. Compared to the IIC method, however, the proposed technique was still able to further reduce the tracking error by over 30% (see Fig. 6 (a2), (b2), Fig. 8 (a2) and Fig. 9). As the rate was further increased to 320 Hz and 400 Hz, the tracking error of the IIC became pronouncedly larger than that of both the MFDIIC and the ODDD-IIC techniques (See Fig. 7, and Fig. 8 (a3), (a4)), with the relative 2-norm and maximum error over 2 and 3 times larger than that of both the MFDIIC and the ODDD-IIC, respectively (see Fig. 9). Such an improvement in tracking precision manifested the advantages of data-driven ILCs: By updating the dynamics "model" instead of using a fixed model—in each iteration, modeling error was eliminated, including that caused by the hysteresis effect of the piezo actuator (albeit small in this experiment). Moreover, dynamics changes of the piezo actuator were also accounted for without trade-off to the tracking performance. Whereas in the IIC method, to account for the quasi-static changes of the system dynamics (before the operation or between iterations), the frequency range for convergence was reduced, resulting in larger tracking error at high-speed. By adjusting the iteration gain at each frequency and in each iteration accordingly (see Corollary 1), the proposed ODDD-IIC exploited the benefits of data-driven for enlarging the convergence frequency range, thereby, further improving the tracking precision: At the triangle rate of 400 Hz, the relative 2-norm and maximum tracking error of the ODDD-IIC were only at 0.75% and 2.5%, respectively, 56% and 55% smaller than those of the MFDIIC, respectively. Moreover, such a precision tracking was attained rather quickly —As shown in Fig. 10, the ODDD-IIC algorithm converged rapidly and reached the limit in only 7 to 8 iterations. As the major frequency components of 400 Hz triangle wave were already higher than the first resonance of the piezo actuator around 780 Hz (see Fig. 3), such a tracking precision—obtained after only 7 or 8 iterations without prior modeling—spoke to the efficacy and efficiency of the proposed technique in high-speed tracking.

2) MULTI-SINE SIGNAL TRACKING: The experimental results on the multi-sine wave tracking results further demonstrated the improvements of the proposed approach in robustness and performance over the constant-gain MFDIIC method. Compared to the triangle wave, the multi-sine wave contained many more high frequency components with larger amplitude (whereas the amplitude of the high-order harmonics of triangle waves dropped rapidly), thereby, was more difficult track. By using the proposed ODDD-IIC technique, precision tracking was still achieved, with both the relative 2-norm and maximum tracking error below 5% (See Fig. 11 (a1), (b1) and Fig. 13). In contrast, when using the MFDIIC method, the 2-norm and maximum tracking errors were 5 and 3 times larger, respectively. Comparison of the tracking error in power spectrum shows this difference in tracking performance was mainly due to the inability of the MFDIIC to track those frequencies around the resonant frequency-those for which the convergence condition of the MFDIIC did not hold (see Fig. 12 top). The comparison of the filtered multi-sine wave tracking further confirmed this observation: After removing these convergence-violation frequencies, the tracking precision of the MFDIIC technique was restored and close to that of the ODDD-IIC technique (see Figs. 11, 12, and 13), with the tracking of the ODDD-IIC still slightly better, particularly around those difficult-to-track frequencies (see Fig. 12 bottom).

Such a difference in the tracking performance, indeed, demonstrated the improvement in robustness/performance through the proposed ODDD-IIC technique: As can be seen from the power spectrum of the NODR in the fifth iteration,  $|\aleph_5(j\omega)|$ , the eight filtered frequency components (see Fig. 14) were all in the frequency range where the NODR exceeded 0.5-the threshold for guaranteeing the convergence of MFDIIC (see Theorem 3). Thus, a larger tracking error occurred when these frequencies were included in the desired trajectory. Whereas, by employing a frequency- and iteration- dependent gain, the proposed technique was able to track these frequency components accurately: As shown in Fig. 14, the iteration gain was reduced when the measured NODR became larger. Therefore, the experimental results showed that the proposed approach provided an effective and efficient means to exploit input-output data while accounting for dynamics variations and external disturbance.

#### V. CONCLUSION

This paper proposed an optimal data-driven difference inversion-based iterative control (ODDD-IIC) method for high-speed tracking in the presence of dynamics changes and random disturbances. The iteration gain was chosen to be frequency- and iteration- dependent, and the convergence of the proposed method under the effect of random disturbance was analyzed. The optimal iteration gain that minimizes the residual tracking error and maximizes the convergence rate was also obtained. It was shown that the proposed ODDD-IIC method improved both robustness and tracking performance over the previous constant-gain MFDIIC method. The experimental implementation on a piezoactuator demonstrated that the proposed ODDD-IIC method achieved superior tracking performance and enhanced robustness over the IIC and the MFDIIC techniques. For the future work, the technique might be extended to more general systems such as Hammerstein system with nonlinear hysteresis behaviors [28], and to MIMO systems [29].

#### REFERENCES

- [1] F. Boeren, A. Bareja, T. Kok, and T. Oomen, "Frequency-domain ilc approach for repeating and varying tasks: With application to semiconductor bonding equipment," *IEEE/ASME Transactions on Mechatronics*, vol. 21, no. 6, pp. 2716–2727, Dec 2016.
- [2] S. Mishra, J. Coaplen, and M. Tomizuka, "Precision positioning of wafer scanners segmented iterative learning control for nonrepetitive disturbances [applications of control]," *IEEE Control Systems Magazine*, vol. 27, no. 4, pp. 20–25, 2007.
- [3] H. W. Yoo, C. J. Kerschner, S. Ito, and G. Schitter, "Iterative learning control for laser scanning based micro 3d printing," *IFAC-PapersOnLine*, vol. 52, no. 15, pp. 169–174, 2019.
- [4] R. B. Warrier and S. Devasia, "Inferring intent for novice human-in-the-loop iterative learning control," *IEEE Transactions on Control Systems Technology*, vol. 25, no. 5, pp. 1698–1710, 2016.
- [5] L. Qiu and E. J. Davison, "Performance limitations of non-minimum phase systems in the servomechanism problem," *Automatica*, vol. 29, no. 2, pp. 337–349, 1993.
- [6] G. Stein, "Respect the unstable," IEEE Control Systems Magazine, vol. 23, no. 4, pp. 12–25, 2003.
- [7] S. Devasia, "Should model-based inverse inputs be used as feedforward under plant uncertainty?" *IEEE Transactions on Automatic Control*, vol. 47, no. 11, pp. 1865–1871, 2002.
- [8] D. Yoon, X. Ge, and C. E. Okwudire, "Optimal inversion-based iterative learning control for overactuated systems," *IEEE Transactions on Control Systems Technology*, 2019.
- [9] S. Devasia, "Iterative control for networked heterogeneous multi-agent systems with uncertainties," *IEEE Transactions on Automatic Control*, vol. 62, no. 1, pp. 431–437, 2016.
- [10] Z. Wang and Q. Zou, "A modeling-free differential-inversion-based iterative control approach to simultaneous hysteresis-dynamics compensation: High-speed large-range motion tracking example," in 2015 American Control Conference (ACC). IEEE, 2015, pp. 3558–3563.
- [11] K.-S. Kim and Q. Zou, "A modeling-free inversion-based iterative feedforward control for precision output tracking of linear time-invariant systems," *IEEE/ASME Transactions on Mechatronics*, vol. 18, no. 6, pp. 1767–1777, 2012.
- [12] S. Tien, Qingze Zou, and S. Devasia, "Iterative control of dynamics-coupling-caused errors in piezoscanners during high-speed afm operation," *IEEE Transactions on Control Systems Technology*, vol. 13, no. 6, pp. 921–931, 2005.
- [13] Y. Jian, D. Huang, J. Liu, and D. Min, "High-precision tracking of piezoelectric actuator using iterative learning control and direct inverse compensation of hysteresis," *IEEE Transactions on Industrial Electron*ics, vol. 66, no. 1, pp. 368–377, 2018.
- [14] J. Lu, Z. Cao, R. Zhang, and F. Gao, "Nonlinear monotonically convergent iterative learning control for batch processes," *IEEE Transactions on Industrial Electronics*, vol. 65, no. 7, pp. 5826–5836, 2018.

- [15] M. Hamidaoui, C. Shao, and S. Haouassi, "A pd-type iterative learning control algorithm for one-dimension linear wave equation," *International Journal of Control, Automation and Systems*, vol. 18, no. 4, pp. 1045– 1052, 2020.
- [16] Q. Liu, S. Tian, and P. Gu, "P-type iterative learning control algorithm for a class of linear singular impulsive systems," *Journal of the Franklin Institute*, vol. 355, no. 9, pp. 3926–3937, 2018.
- Institute, vol. 355, no. 9, pp. 3926–3937, 2018.
  [17] D. Meng and K. L. Moore, "Robust iterative learning control for non-repetitive uncertain systems," *IEEE Transactions on Automatic Control*, vol. 62, no. 2, pp. 907–913, 2017.
- [18] R. Chi, X. Liu, R. Zhang, Z. Hou, and B. Huang, "Constrained datadriven optimal iterative learning control," *Journal of Process Control*, vol. 55, pp. 10–29, 2017.
- [19] D. Meng and K. L. Moore, "Convergence of iterative learning control for siso nonrepetitive systems subject to iteration-dependent uncertainties," *Automatica*, vol. 79, pp. 167–177, 2017.
- [20] R. de Rozario and T. Oomen, "Data-driven iterative inversion-based control: Achieving robustness through nonlinear learning," *Automatica*, vol. 107, pp. 342–352, 2019.
- [21] C.-W. Chen, S. Rai, and T.-C. Tsao, "Iterative learning of dynamic inverse filters for feedforward tracking control," *IEEE/ASME Transactions on Mechatronics*, vol. 25, no. 1, pp. 349–359, 2019.
- [22] P. Janssens, G. Pipeleers, and J. Swevers, "A data-driven constrained norm-optimal iterative learning control framework for lti systems," *IEEE Transactions on Control Systems Technology*, vol. 21, no. 2, pp. 546–551, 2013.
- [23] J. Ren and Q. Zou, "High-speed adaptive contact-mode atomic force microscopy imaging with near-minimum-force," *Review of Scientific Instruments*, vol. 85, no. 7, p. 073706, 2014.
- [24] B. Yan, J. Ren, Y. Liu, H. Huang, X. Zheng, and Q. Zou, "Study of cholesterol repletion effect on nanomechanical properties of human umbilical vein endothelial cell via rapid broadband atomic force microscopy," *Journal of biomechanical engineering*, vol. 139, no. 3, 2017.
- [25] Y.-H. Lee and T.-C. Tsao, "Data-driven ilc for trajectory tracking in nonlinear dynamic systems," in *Dynamic Systems and Control Conference*, vol. 59155. American Society of Mechanical Engineers, 2019, p. V002T14A001.
- [26] Y. Wu and Q. Zou, "Robust inversion-based 2-dof control design for output tracking: piezoelectric-actuator example," *IEEE Transactions on Control Systems Technology*, vol. 17, no. 5, pp. 1069–1082, 2009.
- [27] J. Ren and Q. Zou, "A control-based approach to accurate nanoindentation quantification in broadband nanomechanical measurement using scanning probe microscope," *IEEE Transactions on Nanotechnology*, vol. 13, no. 1, pp. 46–54, 2014.
- [28] J. Liu and Q. Zou, "On superposition of hammerstein systems: Application to simultaneous hysteresis-dynamics compensation," *International Journal of Robust and Nonlinear Control*, vol. 28, no. 14, pp. 4075– 4092, 2018.
- [29] Y. Yan, H. Wang, and Q. Zou, "A decoupled inversion-based iterative control approach to multi-axis precision positioning: 3d nanopositioning example," *Automatica*, vol. 48, no. 1, pp. 167–176, 2012.